Wear 269 (2010) 581–589

Contents lists available at ScienceDirect

Wear

journal homepage: www.elsevier.com/locate/wear

On the transition from mild to severe wear of lubricated, concentrated contacts: The IRG (OECD) transition diagram

R. Bosman*, D.J. Schipper[1]

University of Twente, Drienerloolaan 5, 7500 AE Enschede, The Netherlands

ARTICLE INFO

Article history:
Received 18 February 2010
Received in revised form 21 May 2010
Accepted 10 June 2010
Available online 16 June 2010

Keywords:
Sliding wear
Thermal effects
Wear modeling

ABSTRACT

In this paper the transition from mild wear to severe wear of lubricated, concentrated contacts is dealt with. It is suggested that this transition is thermally induced. The transition from a mild wear to severe adhesive wear occurs when more then 10% of the surface transcends a predefined, critical temperature. A method for determining this critical temperature is presented. Using a BIM based numerical model including the local implementation of Archard's wear law, for the contact pressure and temperature the transition diagram for a model system is calculated and validated by experiments. The transition predicted by numerical calculations is in very good agreement with the experimental determined transition.

1. Introduction

The last decade an increasing demand for smaller machines/components transmitting the same power or more is seen; hence the nominal contact pressures increase. Due to these increasing contact pressures components are operating in the boundary lubrication regime rather than in the full film or mixed lubrication regime. As a result the load is carried by the asperities rather than by the lubricant leaving the adsorbed/reacted boundary layers as the final protection against wear. To be able to design such a component in the most efficient way it is preferred to have beforehand knowledge at which nominal load and velocity the transition from mild wear to adhesive wear will take place. In the late 1980s and early 1990s the International Research Group on Wear of Engineering Materials did a lot of research on this topic, developing "IRG (OECD)" transition diagram [1], three different regions are distinguished as shown in Fig. 1. These regions are distinguished on the bases of the recorded friction-time signals.

Regions I/II indicate the save region at which mild wear will occur. Regions III* and III indicate a region where temporary and respectively permanent severe wear will be present. In this study only the transition from region I/II to III* and I/II to III (thick line in Fig. 1) will be studied, since it is assumed that after passing this transition enhanced wear will occur and the component has failed. Usually the transition diagram for a certain oil/system is based on experiments and lacks a predictive model or gives a relatively simple empirical relation [2–8]. However, it gives a good overview of the parameters influencing the transition to severe adhesive wear, the transition from mild to severe wear shifts to higher values for the load when for instance the viscosity is increased or the sample roughness is decreased. In this paper an attempt is made to predict the transition based on the postulate first made by Blok [9] and later on adapted by Lee and co-workers to include the presumed effect pressure has on the critical temperature [10,11]. Blok originally stated in the late 1930s that the transition from mild to adhesive wear is a thermal phenomenon. Using this assumption the transition diagram is given a more predictive nature. The postulate states that if the contact temperature is higher than the critical temperature of the protective boundary layer, the layer will fail and the system will undergo severe adhesive wear. Blok did not succeed in defining a uniform critical temperature for a defined system. This is probably due to the lack of good thermal models at the time able to deal with contact temperatures in a sufficient degree of detail. van Drogen [12] did succeed in defining a critical temperature for the transition from mild to severe wear using a thermal model taking into account the micro-geometry. However, as discussed in that work the influence of wear is not to be neglected, and was taken into account by adapting the macroscopic geometry by increasing the radius of the bodies in contact. In the current paper the Archard wear law is embedded in the contact model using the local pressure profile as an input. The modeling can be separated in three different parts: (1) contact model, (2)

Abbreviations: BEM, boundary element method; BIM, boundary gradient method; CGM, conjugated gradient method; DC-FFT, diskrete convolution FFT method; FEM, finite element method.

* Corresponding author. Tel.: +31 53 4892476; fax: +31 53 4894784.
E-mail addresses: r.bosman@utwente.nl (R. Bosman), D.J.Schipper@utwente.nl (D.J. Schipper).
[1] Tel.: +3153 4892476.

0043-1648/$ – see front matter © 2010 Elsevier B.V. All rights reserved.
doi:10.1016/j.wear.2010.06.005

Nomenclature

Roman symbols

C_p	specific heat [J/kg °C]
D, D_{ij}	displacement influence coefficient/tensor [m/Pa]
E	elastic modulus [Pa]
F_n, F_{in}, F_{nMesh}	normal force total, incremental, local [N]
g_{ij}	gap [m]
h_{ij}, $h(x, y)$	separation/separation tensor/height loss [m]
I_{discr}, I_c	collection of grid points (all grid points/points in contact)
k	specific wear rate [mm^3/Nm]
K	thermal conductivity [W/M °C]
L	length [m]
N_c	number of elements in contact
$p(x, y)$, p_{ij}	pressure field/tensor [Pa]
Ra	average roughness value ($(1/N)\sum\sum h_{ij} - h_{ij}^{-}$)
r_{ij}	distribution in multidimensional space [m^2/Pa]
S	sliding distance [m]
t_{ij}	search direction [m]
t	time [s]
$T(x, y)$, T_{kl}	thermal influence coefficient/tensor [Θ/Wm^2]
u	surface displacement in normal direction [m]
V	[m/s]
W	wear volume [m^3]
x, y	location of interest [m]
x', x'', y'	location of excitation [m]
Δx, Δy	element size [m]
$\bar{x}_{ij}$	average value of tensor

Greek symbols

ε, ε_{set}	relative error, preset relative error
Θ	temperature rise [°C]
κ	thermal diffusivity [K/ρCp]
μ	coefficient of friction [−]
ν	Poisson ratio [−]
ρ	specific density [kg/m^3]
τ	size of the iteration step [Pa/m]
ϕ	partition factor [−]

thermal model and (3) transition criterion. The different parts will be addressed in this order, starting with the contact model.

2. Contact model

The systems of interest in this study are boundary lubricated thus it is assumed that the contact load is carried by the asperities in contact rather than the lubricant as is assumed in [13]. This assumption makes it feasible to model the contact as a "dry" contact. The effect of the lubricant is only taken into account through a reduction in the coefficient of friction, e.g. the presence of the rather thin protective boundary layers. For dry contact the model used in this study is based on the single loop CGM fist discussed by Polonsky and Keer [14]. In their study a novel method is discussed capable of calculating the elastic contact of large meshes using the B(oundary) I(ntegral) M(ethod) in combination with a multi-level summation method. The efficiency of the model greatly depends on the reduction of iterative loops from two to one, namely only the approach (or rigid body motion) of the bodies relative to each other. Later this method is refined by Liu and Wang by replacing the multi-level summation method by a DC-FFT method, as discussed in [15], increasing the accuracy and calculation speed. This method is based on the basic assumptions that both bodies can be modeled as semi-infinite elastic half-spaces with homogenous properties throughout the bulk. The elastic displacement of the surface due to a pressure field ($p(x, y)$) can now be written as the convolution integral:

$$u(x, y) = -\iint D(x - x', y - y')p(x', y')dx'dy' \tag{1}$$

The influence coefficient ($D(x - x', y - y')$) is given by the Boussinesq formula [16]:

$$D(x, y) = \left(\frac{1 - {\nu_1}^2}{\pi E_1} + \frac{1 - {\nu_2}^2}{\pi E_2}\right)\frac{1}{\sqrt{x^2 + y^2}} \tag{2}$$

Diskretizising Eq. (1) gives at all points of interest (I_{discr}):

$$u_{ij} = \sum D_{i-k,j-l}p_{kl}, \quad (i, j) \in I_{discr} \tag{3}$$

Eq. (3) can be solved using the DC-FFT algorithm if the formula for the influence matrix is known, where

$$D_{ij} = \int_{-\frac{1}{2}\Delta x}^{\frac{1}{2}\Delta x}\int_{-\frac{1}{2}\Delta y}^{\frac{1}{2}\Delta y} D(x_i - x', y_j - y')dx'dy', \quad (i, j) \in I_{discr} \tag{4}$$

The elastic contact problem can now be described by the following equations and inequalities (as discussed in [14]):

$$\sum_{(k,l)\in I_{discr}} D_{i-k,j-l}p_{kl} = h_{ij} + \alpha, \quad (i, j) \in I_c \tag{5}$$

$$p_{ij} > 0, \quad (i, j) \in I_c \tag{6}$$

$$\sum_{(k,l)\in I_{discr}} D_{i-k,j-l}p_{kl} \geq h_{ij} + \alpha, \quad (i, j) \notin I_c \tag{7}$$

with h_{ij} is the original surface separation, α is the rigid body motion and I_c is all grid points in contact.

$$\Delta x \Delta y \sum_{(i,j)\in I_c} p_{ij} = F_n \tag{8}$$

where Δx and Δy are the grid spacing and F_n is the total normal force carried by the contact.

Using a CG based iteration method discussed next, the problem described is solved (for details the reader is referred to [14]). First the displacement of the current pressure guess is computed and from this the current gap:

$$g_{ij} = -u_{ij} - h_{ij}, \quad (i, j) \in I_c \tag{9}$$

The average gap is obtained by:

$$\bar{g} = \frac{1}{N_c}\sum_{(k,l)\in I_c} g_{kl}$$
$$g_{ij} \leftarrow g_{ij} - \bar{g} \tag{10}$$

Here N_c is the current number of elements in contact and I_c are all grid points in the diskretized region where $p_{ij} > 0$. For the new gap the sum is calculated:

$$G = \sum_{(i,j)\in I_c} g_{ij}^2 \tag{11}$$

This value is then used to compute the new conjugate direction t_{ij}:

$$t_{ij} = g_{ij} + \delta\frac{G}{G_{\text{old}}}t_{ij}, \quad (i, j) \in I_c \tag{12}$$

$$t_{ij} = 0, \quad (i, j) \notin I_c \tag{13}$$

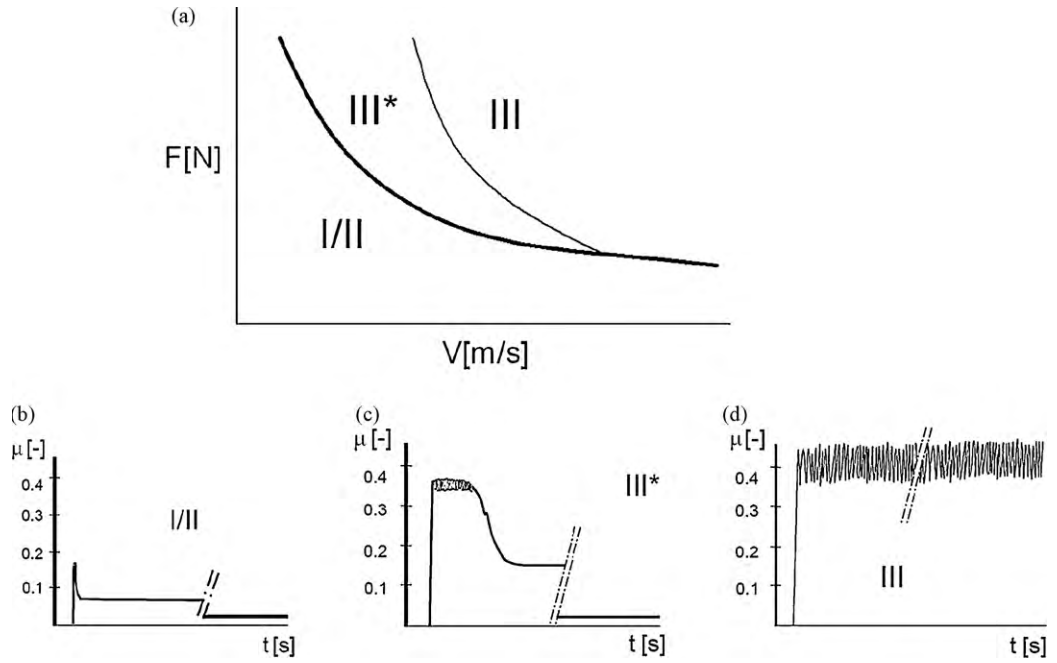

Fig. 1. (a) IRG transition diagram indicating regions I/II (mild wear) and III/III* (severe wear), (b) friction-time signal for wear region I/II, (c) region III* and (d) region III.

The old value of G is now stored for the new iteration ($G_{\text{old}} = G$) and the convolution of D_{ij} and t_{ij} is computed for distribution in the multidimensional space of elemental pressures:

$$r_{ij} = \sum_{(k,l)\in I_{discr}} D_{i-k,j-l} t_{kl}, \quad (i,j) \in I_{discr} \tag{14}$$

$$\bar{r} = \frac{1}{N_c} \sum_{(k,l)\in I_c} r_{kl} \tag{15}$$

$$r_{ij} = r_{ij} - \bar{r}, \quad (i,j) \in I_{discr} \tag{16}$$

The size of the next iteration step is then computed:

$$\tau = \frac{\sum_{(i,j)\in I_c} g_{ij} t_{ij}}{\sum_{(i,j)\in I_c} r_{ij} t_{ij}} \tag{17}$$

The current pressure is stored for error computation:

$$p_{ij}^{\text{old}} = p_{ij}, \quad (i,j) \in I_{discr} \tag{18}$$

Now the pressure is updated:

$$p_{ij} = p_{ij} - \tau t_{ij}, \quad (i,j) \in I_c \tag{19}$$

Next the inequalities of Eq. (6) is enforced setting all $p_{ij} < 0$ equal to 0 after which the overlap is determined:

$$I_{ol} = \left\{ (i,j) \in I_{disrc} : \quad p_{ij} = 0, g_{ij} < 0 \right\} \tag{20}$$

If $I_{ol} = \varnothing$, then δ is set to unity otherwise to zero and the pressures at the overlap are corrected:

$$p_{ij} = p_{ij} - \tau g_{ij}, \quad (i,j) \in I_{ol} \tag{21}$$

Since $\tau > 0$ at every iteration all nodes in I_{ol} will enter I_c enforcing Eq. (6). Next the current contact load is calculated and the error is estimated by enforcing Eq. (8):

$$F_{it} = \Delta x \Delta y \sum_{(i,j)\in I_{discr}} p_{ij} \tag{22}$$

$$p_{ij} = \frac{F_{it}}{F_n} p_{ij}, \quad (i,j) \in I_{discr} \tag{23}$$

$$\varepsilon = \Delta x \Delta y F_n^{-1} \sum_{(i,j)\in I_{discr}} \left| p_{ij} - p^{\text{old}} \right| \tag{24}$$

This iterative loop is repeated until $\varepsilon < \varepsilon_{\text{set}}$, which is set to 10^{-14}. The contact model gives more realistic results by setting a maximum threshold to the contact pressure equal to the hardness of the material which is done in the same way as the restriction in Eq. (6).

To incorporate wear into the contact model a Archard's wear law [17], e.g. wear volume is proportional to the normal load, is applied at a local level. This method is used by many other authors either in combination with FEM or with BEM, see for example: [30–32]. This wear model states that the wear volume is proportional to the load applied and sliding distance through:

$$W = kF_nS \tag{25}$$

where W is the volume loss, k is the specific wear rate and S is the sliding distance. This wear law can also be applied on a local level by replacing the local normal force F_n by the local pressure times the element size. To obtain the loss in height this volume is then divided by the surface of one grid element. Replacing the total sliding distance by the incremental sliding distance (dS) gives:

$$dh(x,y) = kp(x,y)dS \tag{26}$$

Here $dh(x,y)$ is the incremental height loss and $p(x,y)$ the local pressure field acting on the solid. Using the loop shown in Fig. 2 an incremental loading and sliding wear model is realized. In the current study a line contact is used as a model system to validate the theory presented. To simulate this correctly a modification is made to the DC-FFT algorithm for the following reason. The numerical method suggested is limited in the number of elements used. Thus a balance needs to be found between taking into account enough detail of the surface geometry and calculation time. To reduce the number of elements in the direction tangent to the sliding direction (e.g. the largest dimension of the contact) the periodic solution inherent to the FFT formulation is used.

Normally the DC-FFT algorithm is formulated in such a way that it only takes the fist quadrant of the solution as a result of the convolution in the frequency domain, see [18] for details, as the solution

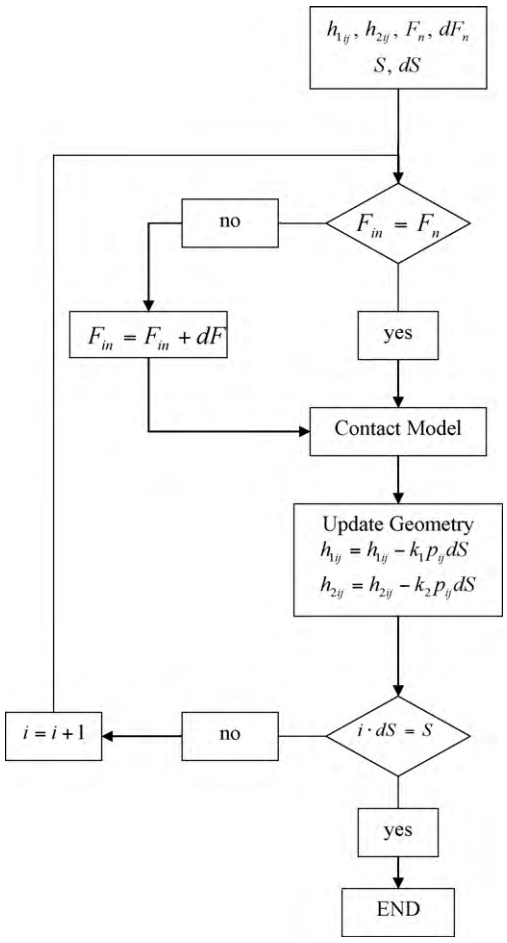

Fig. 2. Incremental load/displacement loop.

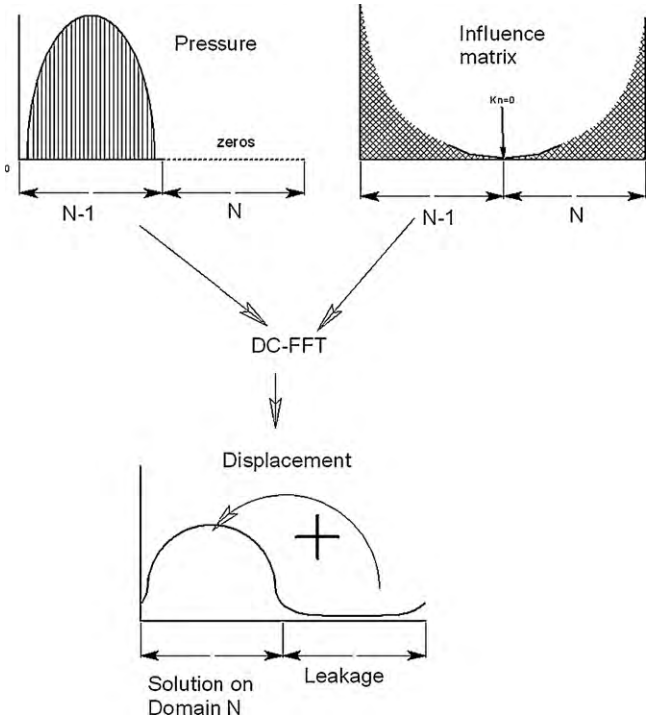

Fig. 3. DC-FFT algorithm and leakage.

in the time/space domain. This is done to compensate for leakage into the domain of interest. If now it is assumed that at both sides of the domain of interest a similar contact is situated (e.g. the contact is semi-periodical) the leakage normally removed can be used to mimic the line contact by adding this to the displacement in the domain of interest, see Fig. 3. To validate this method an example is solved using 3 different methods: (1) original DC-FFT method; (2) DC-FFT with compensation; (3) Hertzian theory. The example consists of a steel cylinder (with the elastic properties given in Table 3) with a radius of 8 mm pressed against a flat plate, resulting in a Hertzian line contact problem. Solving the problem using the classical theory gives a maximum pressure of 1.01 GPa and a semi-contact width of 0.14 mm, which are in good agreement with the results obtained using DC-FFT algorithm with leakage compensation, shown in Fig. 4. The "punch phenomenon" shown in the first figure is consistent for the solution of a pin with the finite length equal to the mesh size. However, this is not the case for the simulation done in this study where only part of the total length of the cylinder is used. For this reason the solution needs to be compensated for this as shown in the right figure. If the DC-FFT algorithm is used without leakage compensation for line contacts the solution is polluted with side effects as is shown in Fig. 4.

3. Thermal model

The thermal model used in this study is also based on the BIM method as discussed in [19]. One of the difficulties of using a thermal model is dealing with the heat partition to the contacting surfaces, which can be approached in different ways. One of the first who dealt with this problem is Blok [20]. This method gives good results for the maximum contact temperature of single contact calculations (e.g. single asperity contact) as is discussed in [21]. However, for a more detailed study of the complete temperature field it is sensible to use a local partitioning method as discussed in [22] and is used in this work.

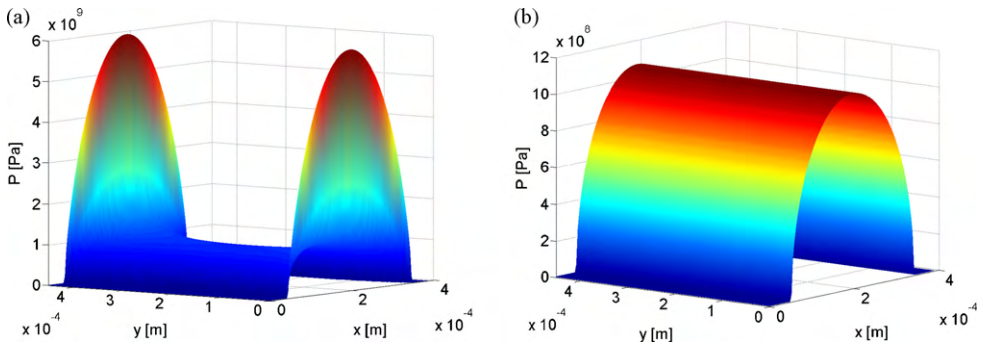

Fig. 4. Pressure field calculated with (a) original DC-FFT algorithm and (b) DC-FFT with compensation for line contact.

The temperature rise of a semi-infinite body can be expressed in the convolution integral as Eq. (1). Here the pressure field is exchanged for the heat source ($q(x, y) = \mu Vp(x, y)$), where it is assumed that the dissipated frictional energy is turned into heat, giving:

$$\Theta(x, y) = -\iint T(x - x', y - y', t)\mu Vp(x', y')dx'dy' \tag{27}$$

Assuming the complete surface is insulated except for the infinite small element $\delta x' \times \delta y''$, on which a uniform square heat source is acting, the influence matrix for a semi-infinite solid can be written as [23]:

$$T(x, y, t) = \int_0^t \frac{1}{\rho C_{cp} 8(\pi\kappa)^{3/2}\tau^{3/2}} \exp \times \left(-\frac{((x' - x'' + U\tau)^2 + (y - y')^2)}{4\kappa\tau}\right) d\tau \tag{28}$$

This can be rewritten for a heat source of finite size ($\Delta x \times \Delta y$) using the following variables [24]:

$$\eta = \frac{x - x'}{2\sqrt{\kappa}\omega} \quad dx' = -2\sqrt{\kappa}\omega d\eta \quad \xi = \frac{y - y'}{2\sqrt{\kappa}\omega} \quad dy' = -2\sqrt{\kappa}\omega d\xi$$
$$V_x' = \frac{V_x\omega}{2\sqrt{\kappa}} \quad \lambda = \frac{z}{2\sqrt{\kappa}\omega} \quad q = \frac{\varphi}{\rho C_p} \quad \omega = \sqrt{\tau}$$
$$d\tau = 2\omega d\omega \quad \eta^0 = \frac{x'' - (x'' - 0.5\Delta x'')}{2\sqrt{\kappa}\omega}$$
$$\eta^1 = \frac{x - (x'' + 0.5\Delta x'')}{2\sqrt{\kappa}\omega} \quad \xi^0 = \frac{y - (y' - 0.5\Delta y)}{2\sqrt{\kappa}\omega}$$
$$\xi^1 = \frac{y - (y' + 0.5\Delta y)}{2\sqrt{\kappa}\omega} \quad m = \frac{x'}{\Delta x} \quad n = \frac{y}{\Delta y}$$

Giving:

$$T(x, y) = \frac{1}{4\sqrt{\pi\kappa}\rho C_p}\int_0^{\sqrt{t}} e^{-\lambda_{mnkl}}(erf(\xi^1_{klmn}) - erf(\xi^0)) (erf(\eta^1 + V_x') - erf(\eta^0 + V'))d\omega \tag{29}$$

The surface temperature distribution can now be computed using Eqs. (29) and (27). However, the heat portioning still needs to be dealt with. This can be done by stating that the temperature fields needs to be continuous over the contact at all contact spots giving:

$$\sum_{(k,l)\in I_{discr}} T^1\phi_{kl}\mu Vp_{kl} = \sum_{(k,l)\in I_{discr}} T^2(1 - \phi_{kl})\mu Vp_{kl} \quad (i, j) \in I_c \tag{30}$$

The inequality described in Eq. (30) containing the partition factor (ϕ) can be solved either directly or using the CGM method. In this work the direct method is chosen since this requires less computational effort. This method requires the computation of the complete influence matrix $T_{i-k,j-l}$ for both bodies which is very memory inefficient, however no iterative loop is needed as is the case for the CGM method. For more details on the way partitioning is handled the interested reader is referred to [21], Section 3.

The influence of incorporating wear in the contact model on the maximum contact temperature is clear in Fig. 5. In this figure the maximum contact temperature is shown for a contact sliding at 1.25 m/s carrying a load of 600 N. The local specific wear rate is set at 1.2×10^{-6} mm^3/Nm. The temperature rise for the model including wear is not only lower but also more gradual and even decreases with increasing time when a constant load is applied. This is due to the fact that wear increases the contact area increasing the thermal conductivity of the total contact and thus lowering the maximum contact temperature (Fig. 6).

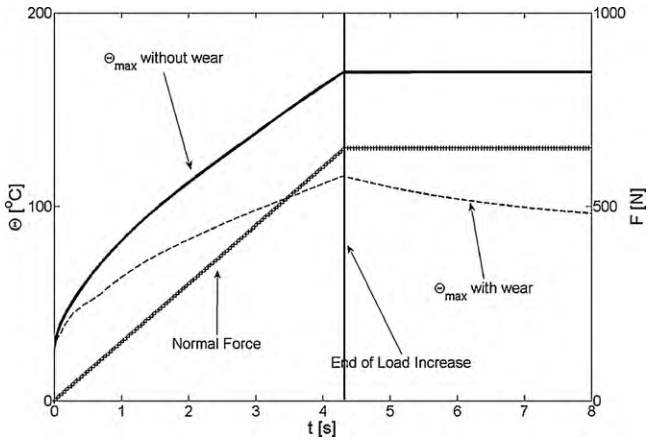

Fig. 5. Calculated maximum temperature during loading of a "non-failure" contact using two different methods: one including wear (Θ_{wear}) and one without (Θ).

4. Transition criterion

As discussed in the introduction Blok postulated that the transition from mild wear to severe wear is thermally induced. However, the temperature calculated along the measured transition using Blok's temperature model was not constant, [6,12]. In [12] the thermal model is expanded to incorporate the flash temperature on asperity level which was not feasible at the time Blok did his work, since no suitable micro-contact models where available at that time. In that work [12] it was shown that the transition from mild to adhesive wear can be predicted by a maximum temperature occurring at the asperity level interface using a asperity based contact model. The temperature criterion used is based on the failure of one single asperity, which may be discussed because the assumption made with respect to the asperity contact model, i.e. the asperities are represented as spheres of which the average temperature is calculated using the theory presented in [22] limits the detail of the model greatly. No distinction is made whether failure occurs at a small micro-contact or a large micro-contact. The influence of the number and size of failing asperities, i.e. the percentage of surface in contact that fails should be taken into account. Therefore, in the current work it is assumed a predefined percentage of the interface transcends the critical temperature at the transition from mild to severe wear. As discussed before the critical temperature needs to be determined to predict the failure of the lubricated contact. The procedure for obtaining this is discussed here briefly, for more details the reader is referred to [12]. An experimental method is used based on the theory of Grew and Cameron [25]. They suggested for determining the critical temperature for a boundary lubricated system using for instance a mineral oil a combination with non-reactive materials should be used to prevent chemo-sorbtion. This statement is based on the assumption that in a contact the temperature is build up from a steady state bulk temperature and a flash temperature. In this situation the flash temperature is of such short duration that the oil (surfactant) is desorbed before it is able to react with the surface preventing chemical reaction layers to form. Therefore, in their study austenitic stainless steel is used which also will be used in this study for determining the critical temperature of the boundary layer. To be able to determine this temperature a test in which as little as possible thermal energy is dissipated is conducted. The procedure consists of a polished stainless steel ball ($Ra < 0.05$ μm) with a radius of 10 mm pressed against a disk with a diameter of 40 mm using a constant normal force of 10 N sliding at a velocity of 0.065 m/s. This test is done on a standardized high temperature pin-on-disk machine.

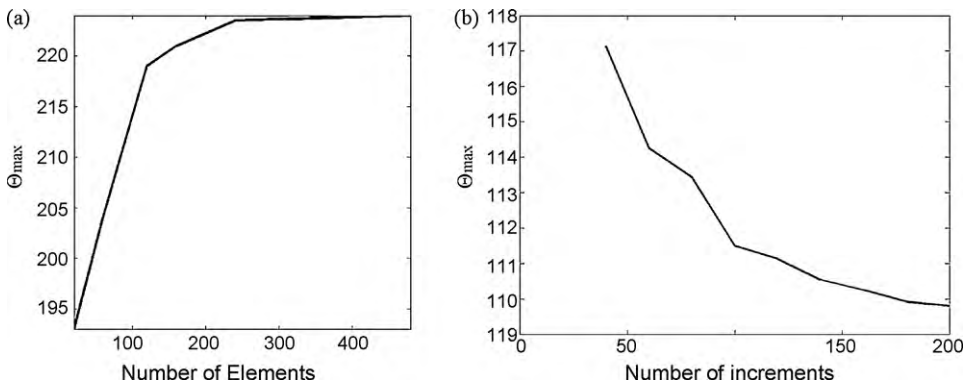

Fig. 6. (a) Maximum contact temperature as a function of the number of elements used and (b) maximum temperature as a function of the number of sliding increments used in the model.

During the test the oil bath temperature is increased until the coefficient of friction "jumps" to a higher value (typically 0.4) as seen in Fig. 7.

Next, a series of experiments is conducted to determine the transition from mild to severe wear. For this a loading sequence needs to be chosen since the way a surface runs in determines greatly the outcome of the transition diagram as is discussed in [26]. For the current work the loading procedure used is one in which new contacting elements are used for every combination of load and sliding velocity. The contact elements consist of a stationary element and a sliding element (as in a normal pin-on-disk set up). First the sliding element (typically a disk) is speeded up to the preset sliding velocity at which point the stationary part is pressed onto it. This procedure is designed to minimize the effect of wear on the transition diagram. However, as will be shown in the next section even after a very small sliding interval wear already has a large influence on the contact. To estimate the mild wear taking place before the transition from mild to severe wear occurs also an approximation is made of the contact area, this is done by optical microscopy of the mild worn surface of the test result closest to the transition from mild to severe wear. If the transition takes place at 750 N and 1.25 m/s the contact area is measured of the test result at a load of 750 N and the velocity prior to the transition velocity. This contact area is then used to estimate a value for the specific wear rate, which can be used in the contact calculations. These tests are preformed on a high load pin-on-disk setup designed in a previous study [12]. The main features of the designed pin-on-disk test rig are given in Table 1.

Table 1
Main features of the high load pin-on-disk setup.

Property	Range	Precision
Normal force	50–1000 N	0.2% at full load-2 N
Friction force	0–500 N	0.05% at full load-0.025 N
Sliding velocity	0.01–22 m/s	0.05% at full load-0.01 m/s
Oil temperature	20–140 °C	1 °C

Due to the non-infinite stiffness of the test rig the normal force signal will not be instantaneous as discussed before but will rather look like a linear loading sequence as shown in Fig. 8. Here a typical loading sequence and additional friction signal are shown for a test resulting in adhesive failure of the contact. For the numerical modeling a linear curve fit is used as input for the normal force as given by the dashed line.

5. Results

To validate the theory described in this paper the transition of a cylindrical pin and a disk sliding under boundary lubrication conditions is calculated and determined experimentally. The oil used in this test is highly refined, light duty mineral white oil with the properties as presented in Table 2. This oil is chosen to assure that the main protection against severe wear is provided by a physical adsorbed layer, which has a relatively low critical temperature, see Fig. 7. First the experimental results, which were all conducted under room temperature and relative humidity between 40% and

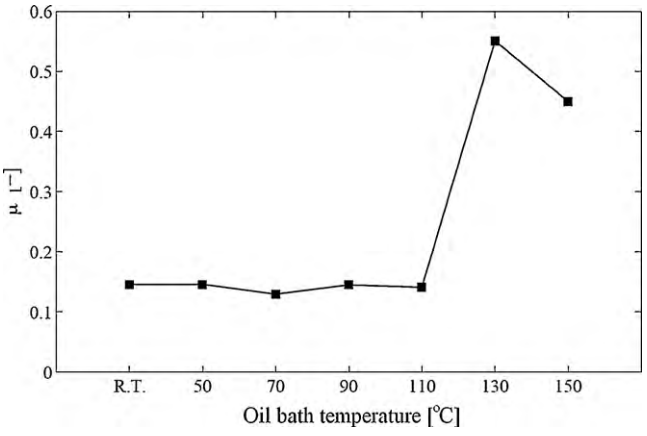

Fig. 7. Typical friction signal of the test procedure for determining the critical temperature. Result shown is for an austenitic stainless steel ball and disk lubricated with highly refined mineral white oil [12].

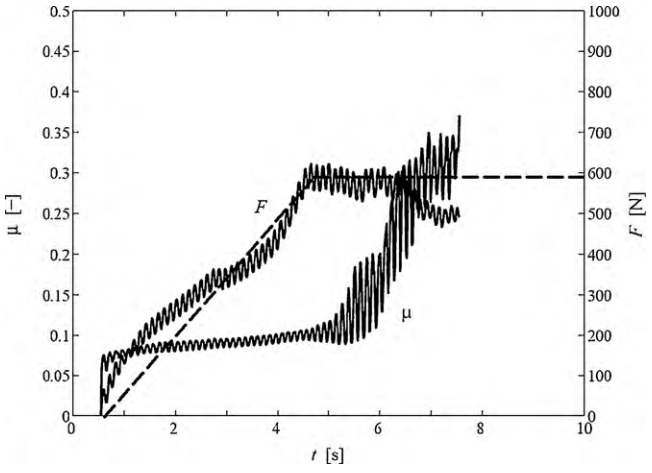

Fig. 8. Typical friction and force measurement of a contact situation with direct failure. Solid line force measured and dashed line force used in the numerical model.

Table 2
Properties of the mineral oil used (Shell Ondina 32).

Density, ρ_d [kg/m^3]	Kinematic viscosity, ν_k [mm^2/s]		Dynamic viscosity, η_0 [mPa s]	
θ = 25 °C	θ = 40 °C	θ = 100 °C	θ = 40 °C	θ = 100 °C
866	32	5	28	4

Table 3
Material properties.

Material	K [W/m °K]	ρ [kg/m^3]	Cp [J/kg °K]	E [GPa]	ν	H [GPa]
AISI 316	17	7780	460	210	0.3	1.1
AISI 52100	45	7800	470	210	0.3	6.6

50%, will be discussed after which the validation of the model is handled.

The critical temperature (Θ_{cr}) is determined by the procedure described in the previous section. The material properties of the AISI 316 used for both contacting elements are presented in Table 3. Using a low load and sliding velocity it was assumed no frictional heating would occur. However, in practice a small increase of the surface temperature was noted and was calculated to be approximately within 15 °C. This together with the result presented in Fig. 7 gives an estimation of the critical temperature of 145 °C.

The next step is determining the transition diagram experimentally. For this purpose a disk with a diameter of 150 mm made of case hardened steel is used in combination with a case hardened cylindrical steel pin with radius 2 mm and length 3.4 mm, resulting in a line contact. The material parameters of the steel are given in Table 3. The surface finish of the disk is grinding resulting in a *Ra* value of 0.27 μM. The pin is grinded and polished so that its relative roughness can be neglected in comparison with the roughness of the disk, giving a rough–smooth surface contact. The transition is determined for the given system according to the procedure discussed in the previous section. The results of these measurements are given in Table 4. The influence of wear on the contact area is clear when comparing the measured contact width ($2b_{\text{meas}}$) with the contact width obtained through elastic perfect plastic calculation ($2b_{\text{roughline}}$). From the measurements a system specific wear rate of 1.2×10^{-6} mm^3/Nm is obtained which is in the range of the values reported in the literature for the system investigated [6–8,27–29]. Since the wear track length on the disk is approximately 100 times the contact width it is assumed that the wear of the system is governed by the wear of the pin. Using the determined k value the contact pressure in time can be calculated.

For the prediction of the transition diagram only a part of the rough surface in contact is used. This part is chosen such that it

Table 4
Measured transitions points and accompanying calculated values.

	Transition points			
Measured				
F [N]	750	600	400	200
V [m/s]	1.25	1.5	2.25	3.75
μ	0.103	0.100	0.091	0.094
$2b_{\text{meas}}$ [μm]	348	364	354	384
Calculated				
$2b_{\text{roughness}}$ [μm]	186	171	153	129
Rel. failure	10.9%	8.7%	12.1%	11.7%
$\Theta_{\max}$ [°C]	157	153	162	160

gives a good representation of the complete surface in contact. The surface topography is measured using an interference microscope with a resolution of 0.816 μm × 0.95 μm and a grid size of 480 × 780 pixels (see Fig. 9).

From this surface a 480 × 480 mesh is used which is then filtered to a 240 × 240 surface with a moving average filter to keep the computational time within limits (e.g. within 1 min for each contact calculation), since every load-sliding cycle is performed incrementally. Since the length of the mesh used is only 0.456 mm and the real length of the pin used is 3.4 mm the force carried is normalized by the mesh length vs. the real length using a normal force of:

$$F_{Nmesh} = F_n \left(\frac{L_{mesh}}{L_{contact}} \right) \tag{31}$$

The load rate applied to the cylindrical pin-on-disk contact is 150 N/s till the preset normal load is reached as is shown in Fig. 8. During the test both the normal force and the friction force are recorded to detect failure of the contact.

If now the sliding and loading process is descritized in steps the increment for every load step can be determined in terms of sliding increment (dS) and load increment (dF). Here only the time interval from onset of loading up to the point the maximum load is reached is descritized. Since in these tests during this period the highest contact temperature will occur, see Fig. 5.

To investigate the sensitivity of the method to the different numerical parameters (e.g. number of elements and number of increment steps) the results of different mesh sizes and increment

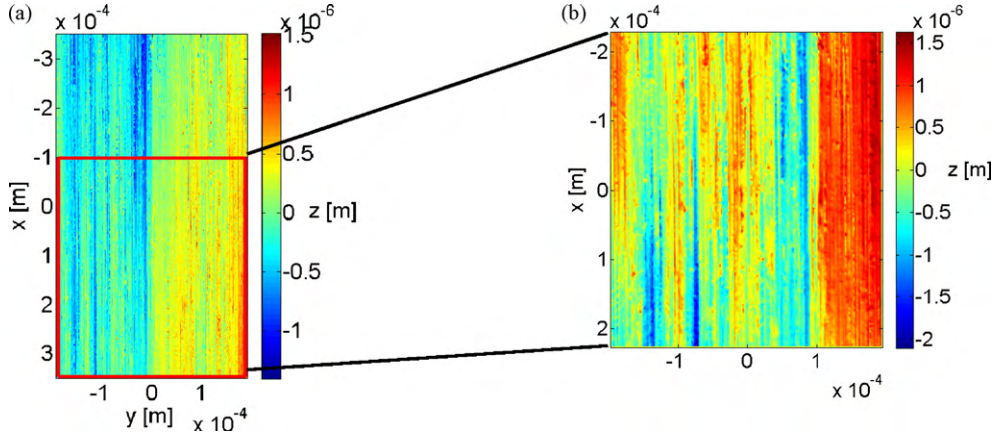

Fig. 9. (a) Measured disk and (b) filtered part of the surface used for the calculations.

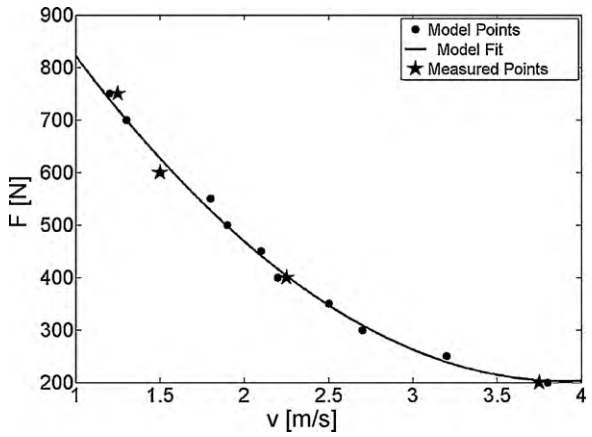

Fig. 10. Transition diagram calculated and measured.

steps were investigated. Fist the number of elements is varied while keeping the load increment equal to 1. As the results in Fig. 6 show increasing the number of elements from 240×240 to 480×480 has little to no effect on the temperature. The number of steps (100) is justified by comparing the results for the lowest sliding velocity and highest load varying the number of increment steps from 20 up to 200. From this analysis it follows that increasing the number of increment steps above 100 does not influence the temperature field. Using the theory discussed before it is now possible to calculate a transition diagram for the pin-on-disk system as a function of normal force and sliding velocity. The calculated maximum contact temperature and percentage of contact area above the critical temperature for the measured transition points are presented in Table 4 and visualized in Fig. 10. From the results it can be concluded that the maximum temperature at the transition from mild to severe wear for the different load is constant and all are within a bandwidth of 10 °C, suggesting that using a thermal failure criterion would give good results. However, the maximum contact temperatures are significantly higher (10%) than the critical temperature determined experimentally. The percentage of the surface which transcends the critical temperature determined experimentally is constant with an average value of approximately 10%.

The results for the temperature and the relative surface failure presented in Table 4 are obtained using the coefficient of friction measured. To give a more predictive nature to the transition diagram during the calculations a coefficient of friction of 0.1 will be used. All measured values are in good agreement with this value. Also the average value of relative surface failure is used as the failure criterion in the numerical calculations, and doing so gives good agreement between the measurements and calculations, as shown in Fig. 10. Here it is seen that the calculated points deviate a little to the smooth line. This is due to the fact that to keep calculation times within realistic values (less than 4 h) a coarse "grid" is used, e.g. the velocity interval is 0.1 m/s while the load is varied between 750 N and 200 N with an interval of 50 N.

To validate if the model can also be applied for systems lubricated with fully formulated oils an attempt was made to determine the critical temperature of a commercial fully formulated CVT oil (oil A) with the properties as given in Table 5. However, it was found

Table 5
Properties of commercial oil A.

Density, ρ_d [kg/m^3]	Kinematic viscosity ν_k [mm^2/s]		Dynamic viscosity, η_0 [mPa s]	
$\theta = 25\,^\circ$C	$\theta = 40\,^\circ$C	$\theta = 100\,^\circ$C	$\theta = 40\,^\circ$C	$\theta = 100\,^\circ$C
862	40	9	35	7

Table 6
Critical temperature determined from the measured transition points for oil A.

	Transition points oil A			
	Room temperature (25 °C)		Elevated temperature (100 °C)	
Measured				
F [N]	700	550	700	400
V [m/s]	3.25	5.75	1.25	1.88
Calculated				
μ	0.1	0.091	0.14	0.14
$2b_{meas}$ [μm]	332	390	321	333
Θ_{max} [°C]	210	230	208	200

that the flash temperature of the base oil was lower than the critical temperature of the lubricant. For this reason it was experimentally impossible to determine the critical temperature of the oil A in the currently study. It was possible to determine the transition points for oil A on the high load setup. The tests where performed at room temperature (25 °C) and elevated temperature (100 °C). The latter is to show that indeed if the environmental temperature is raised the load carrying capacity is reduced due to the fact that the transition temperature is reached at lower load-speed combinations. The results of these tests are given in Table 6 with the corresponding maximum temperature (Θ_{max}) and critical temperature at which more than 10% of the surface in contact has failed ($\Theta_{10\%}$). As can be seen the predicted transition temperature for the different points are within a small interval even for the elevated temperature tests.

The results thus suggest that if one transition point is calculated this can be used to determine the critical temperature of the systems at all points.

6. Conclusions

In this study the temperature is calculated of a smooth cylinder on a rough disk at the transition from mild to severe wear using a contact model that incorporates wear. The results are used in combination with the hypothesis of Blok to predict the transition from mild to severe wear as a function of sliding velocity and normal force for a given system. The numerical models presented are obtained using a contact model and thermal model using adapted DC-FFT and CGM methods to calculate accurate temperature fields for boundary lubricated systems. In the contact model an incremental loading-sliding sequence is incorporated to be able to use Archard's wear model to include mild wear. Including wear gives more realistic results for the contact width and temperature in comparison with non-wear calculations. From the resulting temperature fields it is estimated that if 10% of the surface transcends a critical temperature, which is defined by a standardized protocol, the transition from mild to severe wear occurs. This assumption seems to be arbitrary; however this does not affect the efficiency of the model as long as it predicts a constant "failure percentage" for the transition from mild to severe wear. The relative surface failure criterion is preferred over the classical postulate of the maximum temperature originally stated by Blok. From the calculations in combination with experiments it followed that the maximum temperature at the transition points was significantly higher than the critical temperature found experimentally. The theory presented is experimentally validated and the results from the simulations and experiments are in good agreement with each other.

References

[1] G. Salomon, Failure criteria in thin film lubrication—the irg program, Wear 36 (1976) 1–6.

[2] S. Dizdar, Wear transition of a lubricated sliding steel contact as a function of surface texture anisotropy and formation of boundary layers, Wear 237 (2000) 205–210.
[3] J. Sundh, U. Olofsson, Seizure mechanisms of wheel-rail contacts under lubricated conditions using a transient ball-on-disc test method, Tribology International, 41 (2008) 867–874.
[4] S. Dizdar, S. Andersson, Influence of pre-formed boundary layers on wear transition in sliding lubricated contacts, Wear 213 (1997) 117–122.
[5] S. Dizdar, S. Andersson, Influence of plastic deformation on seizure initiation in a lubricated sliding contact, Wear 232 (1999) 151–156.
[6] A. Begelinger, A.W.J. De Gee, Failure of thin film lubrication—a detailed study of the lubricant film breakdown mechanism, Wear 77 (1982) 57–63.
[7] A. Begelinger, A.W.J. De Gee, Thin film lubrication of sliding point contacts of AISI 52100 steel, Wear 28 (1974) 103–114.
[8] A. Begelinger, A.W.J. De Gee, Failure of thin film lubrication the effect of running-in on the load carrying capacity of thin-film lubricated concentrated contacts, Journal of Lubrication Technology 103 (1981) 103–111.
[9] H. Blok, Seizure delay method for determining the protection against scuffing afforded by extreme pressure lubricants, SAE Journal 44 (1939) 193–204.
[10] S.C. Lee, H. Chen, Experimental validation of critical temperature–pressure theory of scuffing, Tribology Transactions 38 (1995) 738–742.
[11] S.C. Lee, H.S. Cheng, Scuffing theory modeling and experimental correlations, Journal of Tribology 113 (1991) 327–334.
[12] M. van Drogen, The transition to adhesive wear of lubricated concentrated contacts, PhD Thesis, University of Twente, 2005, p. 105, www.tr.ctw.utwente.nl.
[13] A.A. Lubrecht, E. Ioannides, A fast solution of the dry contact problem and the associated sub-surface stress field, using multilevel techniques, Journal of Tribology 113 (1991) 128–133.
[14] I.A. Polonsky, L.M. Keer, A numerical method for solving rough contact problems based on the multi-level multi-summation and conjugate gradient techniques, Wear 231 (1999) 206–219.
[15] S. Liu, Q. Wang, A three-dimensional thermomechanical model of contact between non-conforming rough surfaces, Journal of Tribology 123 (2001) 17–26.
[16] K.L. Johnson, Contact mechanics, Cambridge university Press, Cambridge, 1985.
[17] J.F. Archard, Contact and rubbing of flat surfaces, Journal of Applied Physics 24 (1953) 981–988.
[18] S. Liu, Q. Wang, G. Liu, A versatile method of discrete convolution and FFT (DC-FFT) for contact analyses, Wear 243 (2000) 101–111.
[19] R. Bosman, M.B. de Rooij, Transient thermal effects and heat partition in sliding contacts, Journal of Tribology 132 (2010) 021401.
[20] H. Blok, Theoretical study of temperature rise at surfaces of actual contact under oiliness conditions, Proceedings of the Institution of Mechanical Engineers General Discussion of Lubrication 2 (1937) 222–235.
[21] R. Bosman, Mild microscopic wear in the boundary lubrication regimeGeringer mikroskopischer Verschleiß geschmierter Kontakte in Grenzflächen, Materialwissenschaft und Werkstofftechnik 41 (2010) 29–32.
[22] J. Bos, H. Moes, Frictional heating of tribological contacts, Journal of Tribology 117 (1995) 171–177.
[23] H.S. Carslaw, Conduction of heat in solids, Clarendon press, Oxford, 1959.
[24] B. Vick, Theoretical surface temperatures generated from sliding contact of pure metallic elements, Tribology International 33 (2000) 265–271.
[25] W.J.S. Grew, A. Cameron, Thermodynamics of boundary lubrication and scuffing, Proceedings of the Royal Society of London Series A327 (1972).
[26] D.J. Schipper, R.C. Steenmeijer, A.W.J. De Gee, Variations in the procedure of loading on the load carrying capacity of thin film lubricated concentrated contacts, in: 4th International Tribology Conference, Austrib94, Australia, 1994, pp. 105–112.
[27] A. Begelinger, A.W.J. De Gee, Boundary lubrication of sliding concentrated steel contacts, Wear 22 (1972) 337–357.
[28] A. Begelinger, A.W.J. De Gee, Lubrication of sliding point contacts of AISI 52100 steel—the influence of curvature, Wear 36 (1976) 7–11.
[29] A. Begelinger, A.W.J. De Gee, Thin film lubrication of sliding point contacts formulation of a “collapse parameter”, Institution of Mechanical Engineers, 1977 (Leeds/Lyon).
[30] P. Podra, S. Andersson, Simulating sliding wear with finite element method, Tribology internationa 32 (1999) 71–81.
[31] U. Olofsson, S. Andersson, S. Bjorklund, Simulstion of mild wear in boundary lubricated spherical roller thrust bearings, Wear 241 (2000) 180–185.
[32] G.K. Sfantos, M.H. Aliabadi, Wear simulation using an incremental sliding Boundary Element Method, Wear 260 (2006) 1119–1128.